Gyration tensor based analysis of the shapes of polymer chains in an attractive spherical cage

Handan Arkın and Wolfhard Janke

Citation: J. Chem. Phys. **138**, 054904 (2013); doi: 10.1063/1.4788616
View online: http://dx.doi.org/10.1063/1.4788616
View Table of Contents: http://jcp.aip.org/resource/1/JCPSA6/v138/i5
Published by the American Institute of Physics.

Gyration tensor based analysis of the shapes of polymer chains in an attractive spherical cage

Handan Arkın[1,2,a)] and Wolfhard Janke[1,b)]
[1]*Institut für Theoretische Physik, Universität Leipzig, Postfach 100 920, D-04009 Leipzig, Germany*
[2]*Department of Physics Engineering, Faculty of Engineering, Ankara University, Tandogan, 06100 Ankara, Turkey*

(Received 27 November 2012; accepted 4 January 2013; published online 7 February 2013)

In a recent computational study, we found highly structured conformations for the polymer-attractive sphere model system. Those conformations are of highly ordered spherical shape or form two-dimensional planar, compact to extended, random coil structures. The observed conformations range from desorbed to partially or even completely adsorbed. In order to present their shape characteristics, here we calculate the gyration tensor and related shape descriptors. © *2013 American Institute of Physics*. [http://dx.doi.org/10.1063/1.4788616]

I. INTRODUCTION

The conformational properties of polymers and proteins confined in cages with different geometries are a subject of great interest in polymer science, playing an important role both from a physical and chemical perspective. Theoretical and computational treatments of the adsorption of single polymers provide a complementary approach for basic and applied research into topics such as adhesion[1] to metals[2,3] and semiconductors,[4–6] biomedical implants,[7] and biosensors.[8] The adsorption behavior can also influence cellular motion, drug delivery, and other biological processes. The advances in designing and manipulating biomolecules at solid substrates on the nanoscale open new challenges for potential nanotechnological applications of hybrid organic-inorganic interfaces. As a result, the understanding of biomolecular structure formation near different interfaces has recently been one of the most intensively studied aspects in technology.

Despite numerous detailed numerical studies in the past, due to the complexity introduced for instance by the huge number of sequence possibilities for proteins and different kinds of environments in general, many problems are still open. Recently, some progress has been achieved in this field to understand general properties of conformational behavior of homopolymers and heteropolymers near substrates. This includes theoretical studies which, for example, have been performed to identify the structural phases and the transitions between these using scaling theory,[9,10] mean field functional theory,[11] and numerical simulations of off-lattice models such as coarse-grained polymer chains grafted or not grafted to an attractive surface.[12–17] Therefore, the theoretical treatment of the adsorption of macromolecules within the framework of minimalistic coarse-grained polymer models in statistical mechanics has been a longstanding problem[18,19] that still attracts a lot of interest.[20–27]

In this work, we consider a simple off-lattice coarse-grained polymer model inside an attractive sphere, for which we have recently constructed the finite-temperature phase diagram[28] and investigated the ground-state properties.[29] Here, in the present study, we show that the gyration tensor and the related asphericity and shape anisotropy parameters are powerful combinations to map the conformational pseudophases in detail and to identify the associated typical polymer shapes. In a comparative analysis, a classification of the structures formed in the accompanying adsorption process has been achieved. It is one of the most remarkable results of our study that for different parameter values of the polymer-attractive sphere system, we get conformations that fit perfectly to the inner wall of the sphere with two-dimensional shape.

The rest of the paper is organized as follows. In Sec. II, the model system is described and in Sec. III a brief overview of the employed multicanonical Monte Carlo simulation method and the recorded observables is given. In Sec. IV, we present and discuss our results. Finally, Sec. V concludes the paper with a summary of our findings.

II. MODEL

A. Bead-stick polymer model

The polymer chain is described by a coarse-grained off-lattice model for semiflexible homopolymers, which has also been used for studies of heteropolymers in the frame of the hydrophobic-polar model.[30] As in the lattice models, adjacent monomers are connected by rigid covalent bonds. Thus, the distance is kept fixed and set to unity. The contact interaction of lattice models is replaced by a distance-dependent Lennard-Jones (LJ) potential accounting for short-range excluded volume repulsion and long-range interaction. An additional interaction accounts for the bending energy of any pair of successive bonds. The position vector of the ith monomer, $i = 1, \ldots, N$, is denoted by $\vec{r}_i$. A polymer with N monomers has $N - 1$ bonds of length unity between neighboring monomers

a)E-mail: Handan.Arkin@itp.uni-leipzig.de.
b)E-mail: Wolfhard.Janke@itp.uni-leipzig.de. URL: http://www.physik.uni-leipzig.de/CQT.html.

and $N-2$ bending angles ϑ_i defined through

$$\cos\vartheta_i = (\vec{r}_{i+1} - \vec{r}_i)\cdot(\vec{r}_{i+2} - \vec{r}_{i+1})\,. \tag{1}$$

The LJ potential of nonbonded monomers is of standard 12-6 form. This model was first employed in two dimensions[30] and later generalized to three-dimensional AB proteins,[31,32] partially with modifications taking implicitly into account additional torsional energy contributions of each bond. The energy function for the polymer is thus given by

$$E_p = 4\sum_{i=1}^{N-2}\sum_{j=i+2}^{N}\left(r_{ij}^{-12} - r_{ij}^{-6}\right) + \frac{1}{4}\sum_{i=1}^{N-2}(1-\cos\vartheta_i)\,. \tag{2}$$

In the present study, the bending energy in the second term is chosen to be very weak, so that the polymer is highly flexible.

B. Confining attractive sphere potential

In this work, we assume that the polymer chain is confined inside an attractive sphere of radius R_c, which is a measure of the cage size. The interaction of the polymer chain monomers and the attractive sphere is of van der Waals type, modeled by the usual 12-6 LJ expression. By integrating this interaction over the inner surface, one arrives at

$$E_s = 4\epsilon_c\frac{\pi R_c}{r_i}\left\{\frac{1}{5}\left[\left(\frac{\sigma}{R_c - r_i}\right)^{10} - \left(\frac{\sigma}{R_c + r_i}\right)^{10}\right] - \frac{\epsilon}{2}\left[\left(\frac{\sigma}{R_c - r_i}\right)^{4} - \left(\frac{\sigma}{R_c + r_i}\right)^{4}\right]\right\}, \tag{3}$$

where R_c is the radius of the sphere which is a measure of the cage size, $r_i = (x_i^2 + y_i^2 + z_i^2)^{1/2}$ is the distance of a monomer to the origin and x_i, y_i, z_i are the coordinates of monomers, and $\sigma = 1.0$ and $\epsilon_c = 1.0$ are set to unity. The parameter ϵ in the second term of Eq. (3) defines the attraction strength of the sphere's inner wall and weights the relative importance of intrinsic monomer-monomer and monomer-sphere wall interactions.

III. SIMULATION SETUP

A. Multicanonical method

In order to obtain statistical results of sufficient accuracy, we applied the multicanonical Monte Carlo algorithm[33] (for reviews, see Refs. 34 and 35), where the energy distribution is flattened artificially allowing, in principle, for a random walk of successive states in energy space. This flattening is controllable and therefore reproducible. To this end, the Boltzmann probability is multiplied by a weight factor $W(E)$, which in our case is a function of the energy. Then the multicanonical probability for a state $\{\mathbf{x}\}$ with energy $E(\{\mathbf{x}\})$ reads $p_M(E) = \exp(-E/k_BT)W(E)$. In order to obtain a multicanonical or "flat" distribution, the initially unknown weight function $W(E)$ has to be determined iteratively: In the beginning, the weights $W^{(0)}(E)$ are set to unity for all energies letting the first run be a usual Metropolis simulation, which yields an estimate $H^{(0)}(E)$ for the canonical distribution. This histogram is used to determine the next guess for the weights, the simplest update is to calculate $W^{(1)}(E) = W^{(0)}(E)/H^{(0)}(E)$. Then the next run is performed with probabilities $p_M^{(1)}(E) = \exp(-E/k_BT)W^{(1)}(E)$ of states with energy E, yielding $H^{(1)}(E)$ and $W^{(2)}(E) = W^{(1)}(E)/H^{(1)}(E)$, and so on. The iterative procedure is continued until the weights are appropriate in a way that the multicanonical histogram $H(E)$ is "flat." After having determined accurate weights $W(E)$, they are kept fixed and, following some thermalization sweeps, a long production run is performed, where statistical quantities O are obtained multicanonically, $\langle O\rangle_M = \sum_{\{\mathbf{x}\}} p_M(E(\{\mathbf{x}\}))O(\{\mathbf{x}\})/Z_M$, with the multicanonical partition function $Z_M = \sum_{\{\mathbf{x}\}} p_M(E(\{\mathbf{x}\}))$. The canonical statistics is obtained by reweighting the multicanonical to the canonical distribution, i.e., mean values are computed as $\langle O\rangle = \langle OW^{-1}\rangle_M/\langle W^{-1}\rangle_M$.

B. Observables

In order to check the structural features of conformations or to identify the possible dispersion of conformations because of the interaction with the sphere wall, the gyration tensor of the conformations is calculated, which is defined as

$$S = \frac{1}{N}\begin{pmatrix} \sum_i (x_i - x_{\rm cm})^2 & \sum_i (x_i - x_{\rm cm})(y_i - y_{\rm cm}) & \sum_i (x_i - x_{\rm cm})(z_i - z_{\rm cm}) \\ \sum_i (x_i - x_{\rm cm})(y_i - y_{\rm cm}) & \sum_i (y_i - y_{\rm cm})^2 & \sum_i (y_i - y_{\rm cm})(z_i - z_{\rm cm}) \\ \sum_i (x_i - x_{\rm cm})(z_i - z_{\rm cm}) & \sum_i (y_i - y_{\rm cm})(z_i - z_{\rm cm}) & \sum_i (z_i - z_{\rm cm})^2 \end{pmatrix}. \tag{4}$$

We calculated various shape descriptors derived from the gyration tensor.[36–39] It should be noted that there is no need to calculate the eigenvalues to define the shape descriptors which can be derived from the invariants of the gyration tensor. However, to be as flexible as possible and to get a complete picture, we also computed the eigenvalues of the gyration tensor. Transformation to the principal axis system diagonalizes S,

$$S = \mathrm{diag}(\lambda_1, \lambda_2, \lambda_3), \tag{5}$$

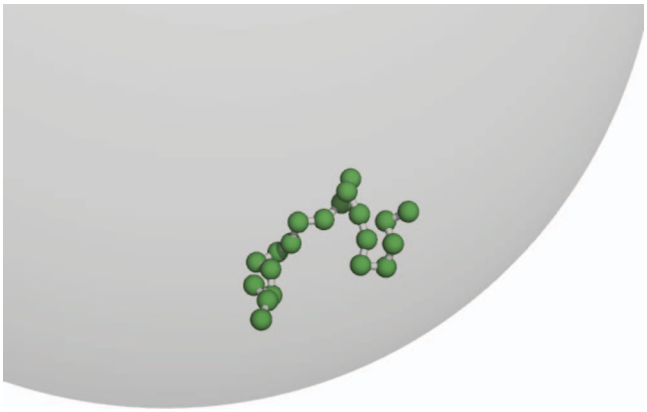

FIG. 1. One of the random conformations which freely moves inside the sphere during the simulation. For the sphere radius, we choose $R_c = 20$ to let the polymer with $N = 20$ monomers circulate freely inside the sphere.

where we assume that the eigenvalues of S are sorted in descending order, i.e., $\lambda_1 \geq \lambda_2 \geq \lambda_3$. The first invariant of S gives the squared radius of gyration,

$$\mathrm{Tr}\, S = \lambda_1 + \lambda_2 + \lambda_3 = R_g^2. \tag{6}$$

The second invariant shape descriptor, or relative shape anisotropy, is defined as

$$\kappa^2 \equiv A_3 = \frac{3}{2}\frac{\mathrm{Tr}\hat{S}^2}{(\mathrm{Tr}S)^2} = 1 - 3\frac{\lambda_1\lambda_2 + \lambda_2\lambda_3 + \lambda_3\lambda_1}{(\lambda_1 + \lambda_2 + \lambda_3)^2}, \tag{7}$$

where $\hat{S} = S - 1/3(\mathrm{Tr}S)E$ with unit tensor E. It reflects both the symmetry and dimensionality of a polymer conformation. This parameter is limited between the values of 0 and 1. It reaches 1 for an ideal linear chain and drops to zero for highly symmetric conformations. For planar symmetric objects, the relative shape anisotropy converges to the value of 1/4.[36–40] The last descriptor, the asphericity parameter b, measures the deviation from the spherical symmetry (recall that λ_1 is the largest eigenvalue):

$$b = \lambda_1 - \frac{1}{2}(\lambda_2 + \lambda_3). \tag{8}$$

C. Computational details

In our simulations, the polymer chain length is $N = 20$ and we set R_c large enough to enclose the polymer inside the sphere. We also have done simulations with different sizes of the sphere ranging from $R_c = 10, 20, 30$. However, to allow the chain to circulate freely inside the sphere and also to reduce the influence on the observables, we eventually set it to 20. Different walls are modeled by varying ϵ between 0.1 and 1.4. The total energy of the system is composed of the pure polymer chain energy and the polymer chain attractive sphere interaction energy. The initial configuration of the polymer chain is randomly generated where the ends have no contact with the sphere attractive wall. One of the random configuration of the simulation is sketched in Fig. 1.

For the determination of the multicanonical weights, we performed 200 iterations with at least 10^5 sweeps each. In the production period, 1×10^8 sweeps were generated to have reasonable statistics for estimating the thermodynamic quantities. Statistical errors are estimated with the standard Jackknife technique.[41,42]

IV. RESULTS AND DISCUSSIONS

The eigenvalues of the gyration tensor measure the extensions in the principle axis system and enable us to define several additional shape parameters of which information about the system can be extracted from that complements the picture. In Fig. 2, the eigenvalues of the gyration tensor and their fluctuations as a function of temperature T for different values of ϵ are displayed. First, one can see that all the eigenvalues are grouped into three phases depending on the attraction strength of the sphere wall ϵ. For small ϵ values, $\epsilon = 0.1, 0.2, 0.3, 0.4, 0.5$, the most compact conformations occur in the low-temperature region with average values of $\langle\lambda_1\rangle \approx 0.75$, $\langle\lambda_2\rangle \approx 0.5$, and $\langle\lambda_3\rangle \approx 0.35$, and the freezing transition temperature is in agreement with that already identified from the specific heat.[28] Additionally, the inflection point of these curves also confirms the temperature which is observed in the specific-heat curve as the collapse transition (random-coil transition). On the other hand, slightly increasing the ϵ value to 0.6 causes an increase of the average $\langle\lambda_1\rangle$ value to about 1.0, $\langle\lambda_2\rangle$ value to 0.75, and a decrease of the average $\langle\lambda_3\rangle$ value to 0.15. By further increasing the ϵ value to $\epsilon = 1.0$, we observe the third group of curves on the plots. Although the freezing transition is hardly affected by the sphere attraction strength, this reveals that there are differently shaped conformations below the freezing transition depending on the sphere attraction strength parameter. Increasing the ϵ parameter, $\langle\lambda_1\rangle$ and $\langle\lambda_2\rangle$ jump to 2.25 and 1.20 at $\epsilon \approx 1.0$, respectively. But $\langle\lambda_3\rangle$ goes to zero, which means that the third group after $\epsilon \approx 1.0$ has two-dimensional shape signaling the layering transition. Above $\epsilon = 1.0$, all other ϵ values yield the typical value zero. From there on, we can conclude that the phase space is separated into three groups which are monolayer, two-layer, and three-layer phases. To support this finding, we also plot the ratio of the greatest eigenvalue to the smallest eigenvalue $\langle\lambda_1/\lambda_3\rangle$ and its temperature derivative in Fig. 3. This ratio takes small values until $\epsilon \approx 1.0$. Above $\epsilon = 1.0$, the ratio of the eigenvalues jumps to higher values signaling that the most pronounced transition is the layering transition which occurs at $\epsilon \approx 1.0$ and separates the conformational spaces of planar conformations which are single-layer and totally adsorbed conformations to the sphere inner wall from two-layer or three-layer and adsorbed spherically compact conformations which are seen at lower ϵ values than $\epsilon \approx 1.0$. This conclusion is also supported by the fluctuations of the ratio $d\langle\lambda_1/\lambda_3\rangle/dT$ shown in Fig. 3(b). As a result, the eigenvalues of the gyration tensor and their fluctuations establish the phases below the freezing transition, which are the most pronounced layering transitions.

Since the asphericity parameter b is a linear combination of the eigenvalues of the gyration tensor, the same typical behavior as in $\langle\lambda_1\rangle$ occurs also in the mean value of the asphericity parameter $\langle b\rangle$ and in its temperature derivative [Figs. 4(a)

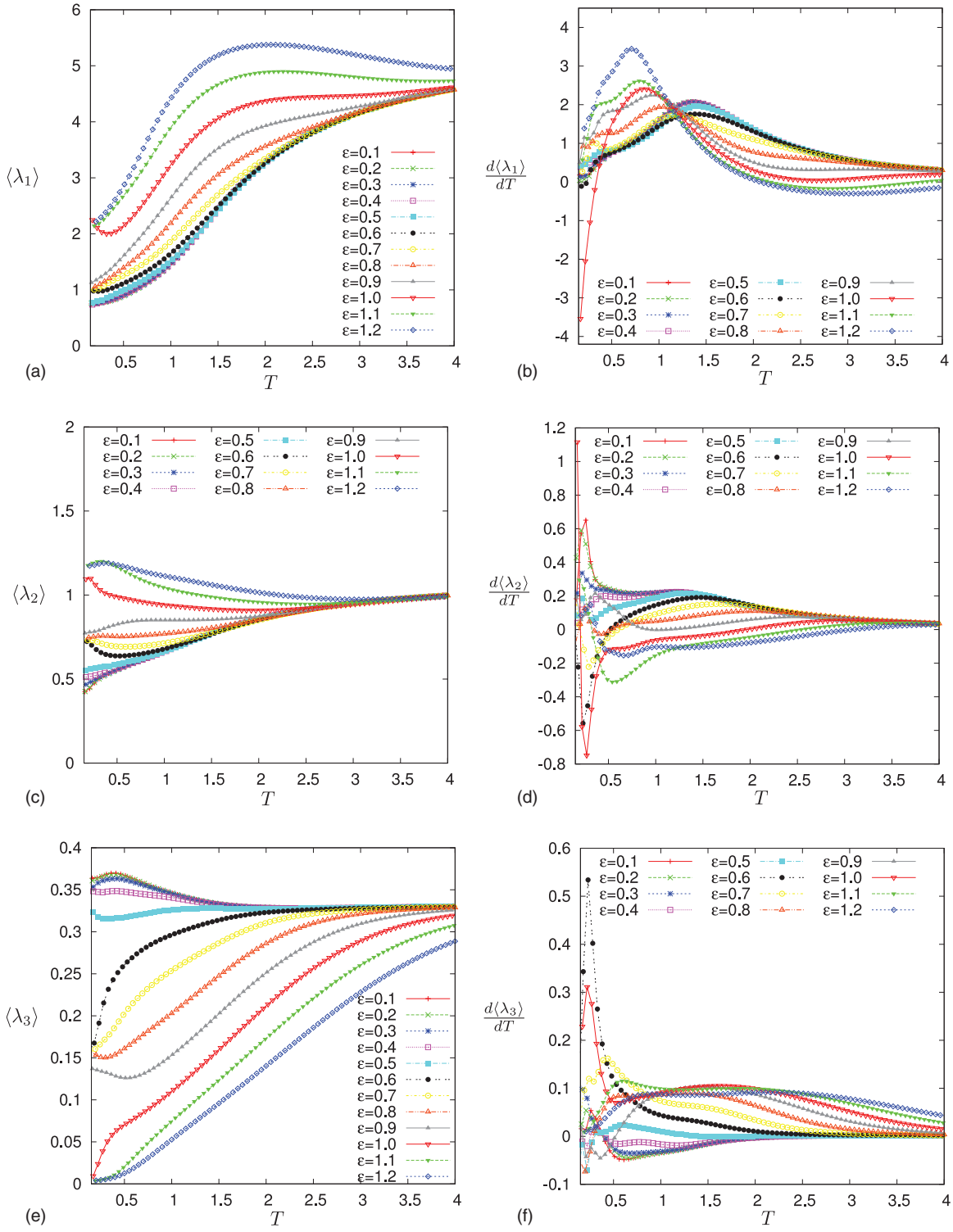

FIG. 2. (a)–(f) The canonical expectation values of the three eigenvalues $\langle\lambda_1\rangle$, $\langle\lambda_2\rangle$, and $\langle\lambda_3\rangle$ of the gyration tensor and their temperature derivatives for different attraction strength values ϵ.

and 4(b)]. The three groupings for different ϵ values can also be seen here. For small values of ϵ, the asphericity parameter is smaller, because the conformations are almost spherically symmetric, but for larger ϵ values it increases and at $\epsilon \approx 1.0$ it jumps to higher values significantly.

More details of the shape characteristics are revealed by the relative shape anisotropy which is shown in Fig. 5. In our simulations, the compact, spherically-shaped conformations reach an average value of $\langle\kappa^2\rangle \approx 0.05$ for smaller attraction strength ($\epsilon = 0.1, 0.2, 0.3, 0.4, 0.5$). Increasing the attraction strength also causes an increase in this parameter signaling that the conformations are not spherically symmetric anymore. Rather, two-layer structures dominate in this regime ($\langle\kappa^2\rangle \approx 0.16$). Further increasing ϵ, we detect at $\epsilon = 1.0$ the

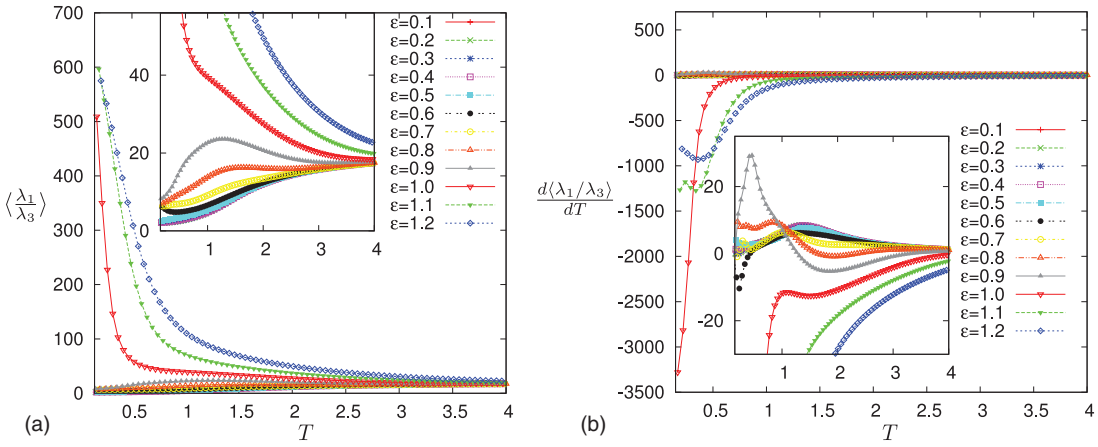

FIG. 3. (a) The ratio of the greatest eigenvalue to the smallest eigenvalue $\langle \lambda_1/\lambda_3 \rangle$ and (b) its temperature derivative for different attraction strength values ϵ. The insets give a magnified view of the same data over a much smaller y-range.

layering transition where $\langle \kappa^2 \rangle$ reaches approximately a value of 0.32. The relative shape anisotropy parameter has two minima in the temperature dependence, one at $\epsilon = 0.6$ and one at $\epsilon = 1.0$, where these points signal the phase transition points.

Further important results are illustrated in Fig. 6, where we plot the eigenvalue distributions of the gyration tensor for low-temperature conformations for (a) $\epsilon = 0.1$, (b) $\epsilon = 0.4$, (c) $\epsilon = 0.7$, and (d) $\epsilon = 1.0$. For $\epsilon = 0.1$ and 0.4, the eigenvalues are nearly equal to each other. There are no significant differences because these values correspond to spherically symmetric shapes or three-layered shapes, which are also near to spherical shape. On the other hand, as it was observed before that the transition point is at $\epsilon \approx 0.6$, the plot for $\epsilon = 0.7$ shows the tendency of increasing the values of λ_1 and λ_2 and decreasing of λ_3. For $\epsilon = 1.0$, it can be seen that λ_3 vanishes to zero and the other eigenvalues are increasing to higher values. This shows us that the layering transition is a topological transition from 3D to 2D polymer conformations.

The phase structure derived from specific-heat curves (data not shown) and from all of the structural observables is summarized in the pseudophase diagram in the ϵ-T plane of Fig. 7. The boundaries in the diagram separate the different structural pseudophases labeled by a letter code adopted from Refs. 12 and 27. Representative conformations are also displayed in the figure. In the pseudophase diagram, the temperature increases from bottom to top and the attraction strength of the sphere inner wall increases from left to right. For low attraction strength, the polymer behaves similarly to a free polymer where below the freezing transition compact conformations (desorbed compact, DC) are identified and above the transition globular (desorbed globular, DG) ones. At higher temperatures, a second transition signals the globular to desorbed expanded (DE) or in other words random-coil transition. Increasing the attraction strength leads to increasing the temperature of the adsorption transition. This transition separates desorbed conformations and adsorbed conformations. In the adsorbed region below the collapse transition, there is an adsorbed globular (AG) phase where the conformations look like a drop on the surface. At even higher temperature and ϵ, there is the partially adsorbed extended phase (AE2). Except adsorption, collapse, and freezing

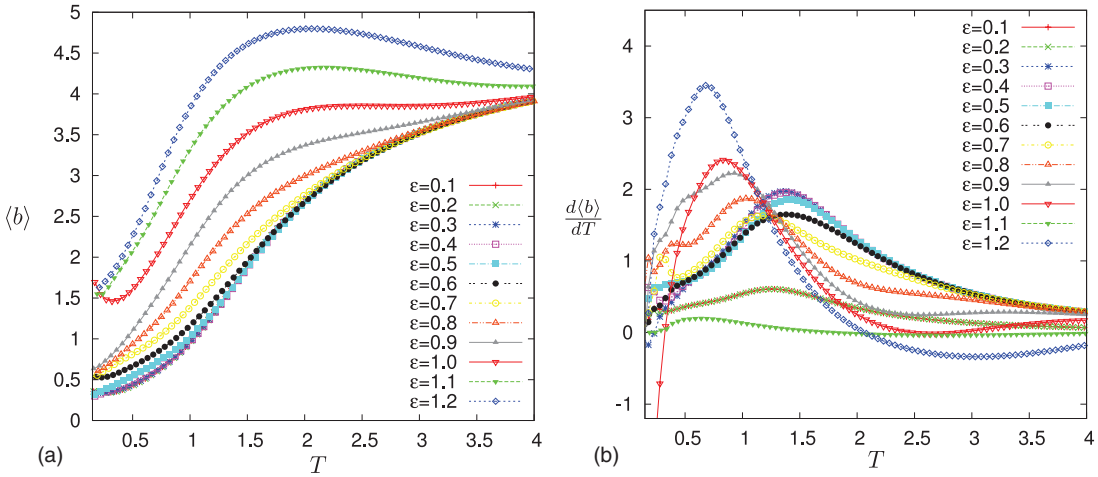

FIG. 4. (a) The canonical expectation value of the asphericity parameter $\langle b \rangle$ and (b) its temperature derivative for different attraction strength values ϵ.

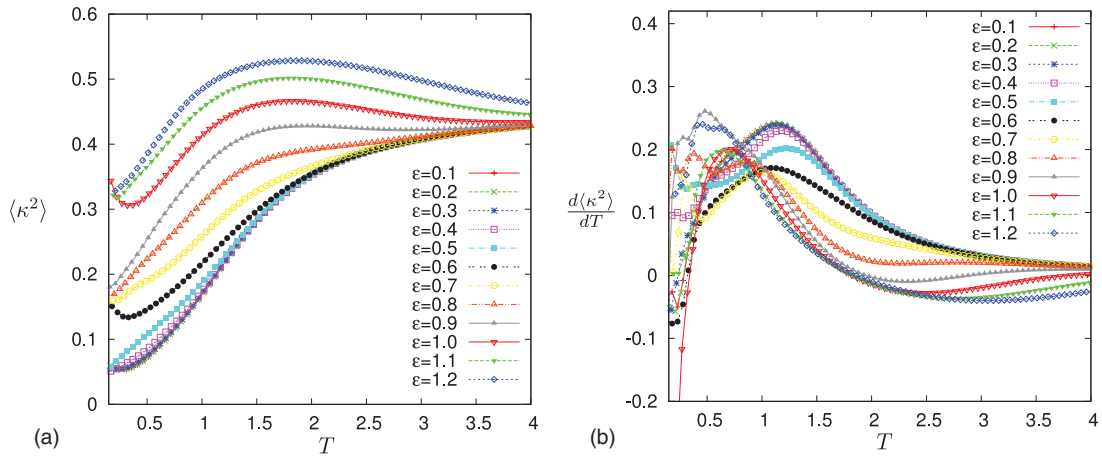

FIG. 5. (a) The canonical expectation value of the relative shape anisotropy parameter $\langle\kappa^2\rangle$ and (b) its temperature derivative for different attraction strength values ϵ.

transitions, the most pronounced transition which we detected is the layering transition which comes into play at $\epsilon \approx 1.0$. This transition separates the conformational spaces of planar conformations which are single-layer and totally adsorbed conformations to the sphere inner wall (AC1, AE1) from two-layer (AC2) or three-layer (AC3), and adsorbed spherically compact (AC4) conformations which are seen at ϵ values smaller than $\epsilon \approx 1.0$. The latter structures which are determined from the shape parameters occur when the attraction strength is not yet strong enough to induce one-layer compact structures but sufficiently high to favor polymer-sphere wall contacts.

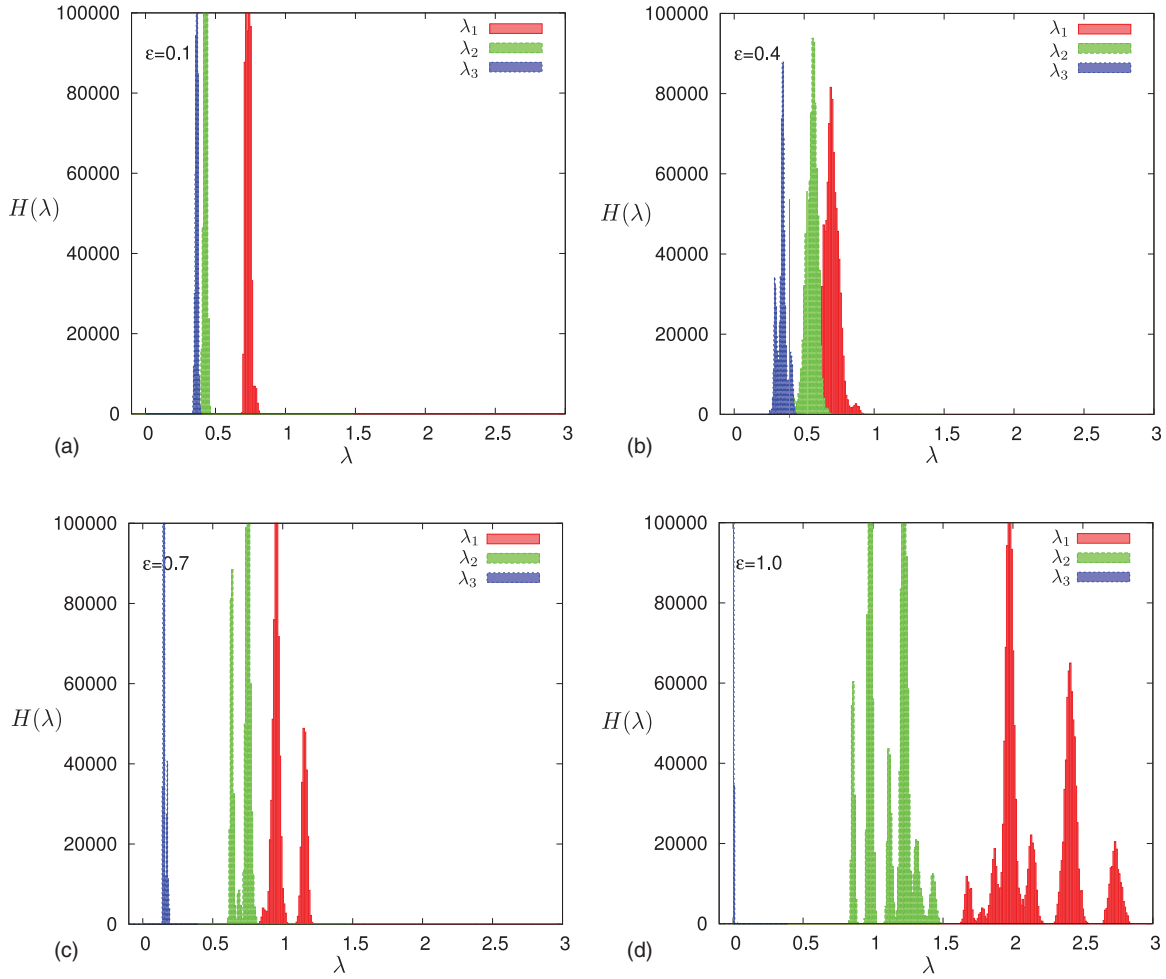

FIG. 6. The eigenvalue distributions of the gyration tensor for low-temperature conformations for (a) $\epsilon = 0.1$, (b) $\epsilon = 0.4$, (c) $\epsilon = 0.7$, and (d) $\epsilon = 1.0$.

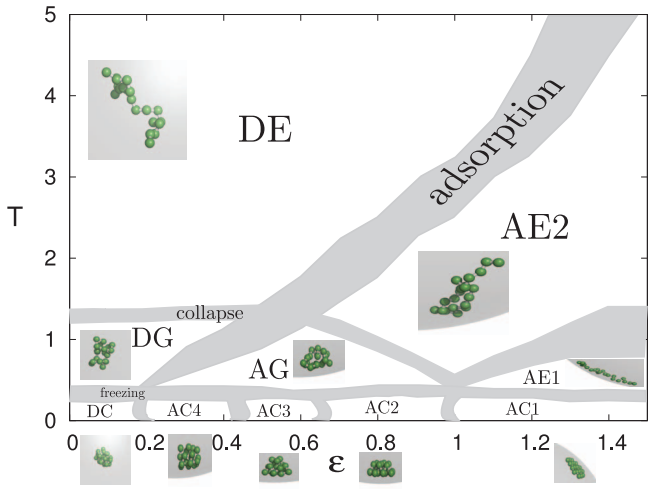

FIG. 7. The pseudophase diagram of the polymer-attractive sphere system as obtained in extensive multicanonical simulations, parametrized by attraction strength ϵ and temperature T. The boundaries separate the individual conformational phases. The band width, which reflects the transition regions, shows the variation of the peaks of temperature derivatives of different structural observables, which have been analyzed simultaneously. The phases labeled with an "A/D" are adsorbed/desorbed. DE, DG, and DC label the desorbed phases of expanded, globular, and compact/crystalline conformations, respectively. AE1 denotes completely adsorbed and AE2 partially adsorbed expanded structures. AG stands for the adsorbed globular regime and the compact/crystalline structures occur in various topologies with a different number of layers: AC4—adsorbed spherically symmetric, AC3—adsorbed three-layer structures, AC2—adsorbed two-layer structures, and finally AC1—adsorbed single-layer structures. The representative conformations are also compiled in the figure.

V. CONCLUSION

In this paper, we have studied the structure formation of a coarse-grained off-lattice polymer model inside an attractive sphere and we found highly structured conformations in the phase space depending on the temperature and attraction strength. Those conformations are of highly ordered spherical shape or form two-dimensional planar, compact to extended, random coil structures. The observed conformations range from desorbed to partially or even completely adsorbed. In order to present their shape characteristics, we calculated the gyration tensor and related shape descriptors. We found that at low attraction strength, the conformations are spherically symmetric compact structures, which is also the main property of a freely moving polymer without being in interaction with its environment. The mean values of structural parameters such as the asphericity $\langle b \rangle$ and the relative shape anisotropy $\langle \kappa^2 \rangle$ show that on average the structures reach a spherical compact shape. But it should be noted that even in the low-temperature regime some fluctuations occur and the conformations are elongated from the perfect spherical shape. The presence of an attractive sphere strongly affects the conformations of the polymer at the interface for stronger interactions. The monomer-monomer interactions and the monomer-sphere interactions compete with each other and this competition results in different phases depending on the attraction strength. Moreover, we found a detectable grouping in the mean values of the eigenvalues of the gyration tensor and in the structural parameters such as $\langle \kappa^2 \rangle$ and the asphericity parameter $\langle b \rangle$ indicating the layering transitions. Increasing the attraction strength causes three-layer and two-layer structures whose first layer is adsorbed to the sphere inner wall. For sufficiently high attraction strengths, we observe the formation of single-layer structures which perfectly fit to the spherical confinement. At the end, we summarize all our findings coming from different structural observables and their temperature derivatives in the phase diagram in the ϵ-T plane.

ACKNOWLEDGMENTS

We wish to thank Viktoria Blavatska, Martin Marenz, Monika Möddel, and Johannes Zierenberg for useful discussions. H.A. acknowledges support by the Alexander von Humboldt Foundation under the Experienced Researcher Fellowship Programme. W.J. thanks the German Research Foundation, Deutsche Forschungsgemeinschaft (DFG) for support under Grant Nos. JA483/24-3 and SFB/TRR 102 project B04. The computer time for the Monte Carlo simulations was provided by NIC, Forschungszentrum Jülich under Grant No. hlz17, which we gratefully acknowledge.

[1] S. Walheim, E. Schaffer, J. Mlynek, and U. Steiner, Science **283**, 520 (1999).
[2] S. Brown, Nat. Biotechnol. **15**, 269 (1997).
[3] R. Braun, M. Sarikaya, and K. Schulten, J. Biomater. Sci., Polym. Ed. **13**, 747 (2002).
[4] S. R. Whaley, D. S. English, E. L. Hu, P. F. Barbara, and A. M. Belcher, Nature (London) **405**, 665 (2000).
[5] K. Goede, P. Busch, and M. Grundmann, Nano Lett. **4**, 2115 (2004).
[6] M. Bachmann, K. Goede, A. G. Beck-Sickinger, M. Grundmann, A. Irbäck, and W. Janke, Angew. Chem., Int. Ed. **49**, 9530 (2010).
[7] E. Nakata, T. Nagase, S. Shinkai, and I. Hamachi, J. Am. Chem. Soc. **126**, 490 (2004).
[8] R. F. Service, Science **270**, 230 (1995).
[9] E. Eisenriegler, K. Kremer, and K. Binder, J. Chem. Phys. **77**, 6296 (1982).
[10] Z. Usatenko, J. Stat. Mech.: Theory Exp. **2006**, P03009.
[11] J. Forsman and C. E. Woodward, Phys. Rev. Lett. **94**, 118301 (2005).
[12] M. Möddel, M. Bachmann, and W. Janke, J. Phys. Chem. B **113**, 3314 (2009).
[13] M. Möddel, W. Janke, and M. Bachmann, Phys. Chem. Chem. Phys. **12**, 11548 (2010).
[14] M. Möddel, W. Janke, and M. Bachmann, Macromolecules **44**, 9013 (2011).
[15] A. Milchev and K. Binder, J. Chem. Phys. **117**, 6852 (2002).
[16] I. Gurevitch and S. Srebnik, Chem. Phys. Lett. **444**, 96 (2007); J. Chem. Phys. **128**, 144901 (2008).
[17] T. Vogel and M. Bachmann, Phys. Rev. Lett. **104**, 198302 (2010).
[18] E. Eisenriegler, *Polymers Near Surfaces* (World Scientific, Singapore, 1993).
[19] G. J. Fleer, M. A. Cohen Stuart, J. M. H. M. Scheutjens, T. Cosgrove, and B. Vincent, *Polymers at Interfaces* (Chapman and Hall, London, 1993).
[20] H. W. Diehl and M. Shpot, Nucl. Phys. B **528**, 595 (1998).
[21] A. Sikorski, Macromol. Theory Simul. **11**, 359 (2002).
[22] M. Bachmann and W. Janke, Phys. Rev. Lett. **95**, 058102 (2005).
[23] M. Bachmann and W. Janke, Phys. Rev. E **73**, 041802 (2006).
[24] M. Bachmann and W. Janke, Phys. Rev. E **73**, 020901(R) (2006).
[25] K. Binder, J. Baschnagel, M. Müller, W. Paul, and F. Rampf, Macromol. Symp. **237**, 128 (2006).
[26] J. Luettmer-Strathmann, F. Rampf, W. Paul, and K. Binder, J. Chem. Phys. **128**, 064903 (2008).
[27] S. Karalus, W. Janke, and M. Bachmann, Phys. Rev. E **84**, 031803 (2011).
[28] H. Arkın and W. Janke, Phys. Rev. E **85**, 051802 (2012).
[29] H. Arkın and W. Janke, J. Phys. Chem. B **116**, 10379 (2012).
[30] F. H. Stillinger, T. Head-Gordon, and C. L. Hirshfeld, Phys. Rev. E **48**, 1469 (1993); F. H. Stillinger and T. Head-Gordon, *ibid.* **52**, 2872 (1995).
[31] A. Irbäck, C. Peterson, F. Potthast, and O. Sommelius, J. Chem. Phys. **107**, 273 (1997).

[32]A. Irbäck, C. Peterson, and F. Potthast, Phys. Rev. E **55**, 860 (1997).
[33]B. A. Berg, and T. Neuhaus, Phys. Lett. B **267**, 249 (1991); Phys. Rev. Lett. **68**, 9 (1992); W. Janke, Int. J. Mod. Phys. C **3**, 1137 (1992).
[34]B. A. Berg, "Introduction to multicanonical Monte Carlo simulations," in *Fields Institute Communications, Monte Carlo Methods*, Vol. 26, edited by Neal Madras (Co-published by the AMS and Fields Institute, 2000), p. 1.
[35]W. Janke, Physica A **254**, 164 (1998).
[36]K. Solc and W. H. Stockmayer, J. Chem. Phys. **54**, 2756 (1971).
[37]D. N. Theodorou and U. W. Suter, Macromolecules **18**, 1206 (1985).
[38]V. Blavatska and W. Janke, J. Chem. Phys. **133**, 184903 (2010).
[39]J. Vymětal and J. Vondrášek, J. Phys. Chem. A **115**, 11455 (2011).
[40]V. Blavatska and W. Janke, J. Chem. Phys. **136**, 104907 (2012).
[41]B. Efron, *The Jackknife, the Bootstrap and Other Resampling Plans* (Society for Industrial and Applied Mathematics (SIAM), Philadelphia, 1982).
[42]W. Janke, "Monte Carlo methods in classical statistical physics," in *Computational Many-Particle Physics*, Lecture Notes in Physics Vol. 739, edited by H. Fehske, R. Schneider, and A. Weiße (Springer, Berlin, 2008), pp. 79–140.